

## Jamming pattern in a two-dimensional hopper

Kiwing To<sup>1,\*</sup> and Pik-Yin Lai<sup>1,2</sup>

<sup>1</sup>*Institute of Physics, Academia Sinica, Taipei, Taiwan 115, Republic of China*

<sup>2</sup>*Department of Physics and Center for Complex Systems, National Central University, Chung-Li, Taiwan 320, Republic of China*

(Received 21 January 2002; published 29 July 2002)

We perform granular flow experiments using metal disks falling through a two-dimensional hopper. When the opening of the hopper  $d$  is small, jamming occurs due to formation of an arch at the hopper opening. We study the statistical properties of the horizontal component  $X$  and the vertical component  $Y$  of the arch vector that is defined as the displacement vector from the center of the first disk to the center of the last disk in the arch. As  $d$  increases, the distribution function of  $X$  changes from a steplike function to a smooth function while that of  $Y$  remains symmetrical and peaked at  $Y=0$ . When the arch vectors are classified according to the number of disk  $n$  in the arch, the mean value  $\langle n \rangle$  is found to increase with  $d$ . In addition, the horizontal component  $X_n$  and the absolute value of the vertical component  $|Y_n|$  in each class have mean values increasing with  $n$ . Regarding the arch as a trajectory of a restricted random walker, we derive an expression for the probability density function  $a_n(X)$  of forming an  $n$ -disk arch. The statistics ( $\langle n \rangle$ ,  $\langle X_n \rangle$ ,  $\langle |Y_n| \rangle$  and the fraction  $g_d(n)$  of  $n$ -disk arches) of the arches generated by  $a_n(X)$  agree with those found in the experiment.

DOI: 10.1103/PhysRevE.66.011308

PACS number(s): 45.70.Qj, 45.70.Mg, 45.70.Vn

### I. INTRODUCTION

Although hoppers and silos are very common industrial and agricultural appliances, the dynamics of the granular materials flowing inside them is not clearly understood (see Ref. [1] and reference therein). The flow properties of granular materials is rather complex and there have been attempts to understand the basic physics of these systems both experimentally and theoretically [2–6]. It is common knowledge that the flow rate of grains through a hopper increases with the size of the hopper opening. However, when the hopper opening is comparable to the size of the grains, flow rate cannot be measured because jamming occurs unpredictably [7]. Once jamming takes place, no more grain can flow through the hopper unless perturbed externally. Jamming is one of the peculiar processes exhibited by granular systems whose dynamical behavior is poorly understood [8,9]. Because jamming is a random process, it is natural to take a statistical approach to analyze the phenomenon. Recently, the flow of monodisperse disks under gravity in a two-dimensional (2D) hopper has been studied. By analyzing the disk configuration in each jamming event, To *et al.* found that the jamming probability observed in their experiments could be obtained using a restricted random walk model (RRWM) [10]. This model regards the jamming process as the formation of a stable arch at the hopper opening. The effect of the hopper is to let go those arches that are smaller than the opening. When an arch bigger than the opening is formed, if it is stable and strong enough it blocks and supports the disks above. Then the probability that jamming occurs should be related to the probability of forming an arch at the opening. When the configuration of the disks in the arch is described as the trajectory of a random walker, the arch forming probability and thus the jamming probability can be estimated. In this paper we report on the results of a

further investigation of jamming in a 2D hopper. A description of the experimental aspect, a brief summary, and the general properties of the data obtained will be given in the following section. Then the RRWM will be presented and its prediction will be compared to the statistics of the arch found in each jamming event. A summary and outlook will be given at the end.

### II. EXPERIMENT

#### A. Setup and procedures

The details of the experimental setup have been given in Ref. [10]. In brief, 200 monodisperse 3-mm-thick metal disks of diameter  $D=5$  mm are made to fall through a 4-mm gap between an aluminum plate and a transparent plexiglass. A pair of metal plates (MP, FP) within the same gap forms the inclined walls of the 2D hopper. These plates are cut with an angle  $\phi=60^\circ$  with respect to the horizontal axis and their relative distance determines the opening  $R$  of the hopper (see Fig. 1). The hopper is mounted on a vertical rotating stage (i.e., the rotation axis  $W$  is along the horizontal direction) such that the symmetry axis of the hopper is perpendicular to  $W$ . The experiment starts with the hopper at the upright position when disks in the hopper are falling towards the hopper opening. Then the hopper is rotated upside down so that all of the disks fall back into the hopper and the experiment repeats when the hopper is rotated back to the upright position again. At a particular  $d \equiv R/D$ , we repeat the experiment  $N_t$  times, record the number  $N_a$  of jamming event and obtain the jamming probability  $J(d) \equiv N_a/N_t$ . For each jamming event, an image of the hopper, as shown in Fig. 2(a), is taken using a charge-coupled device camera and a frame grabber. From each of the captured images, we locate the positions of the disks and determine the number of disks  $n$  in the arch. We shall call the arch consisting of  $n$  disks as an  $n$ -disk arch and denote the number of jamming events with  $n$ -disk arch by  $N_n$ . Since the relevant length

\*Electronic address: ericto@gate.sinica.edu.tw

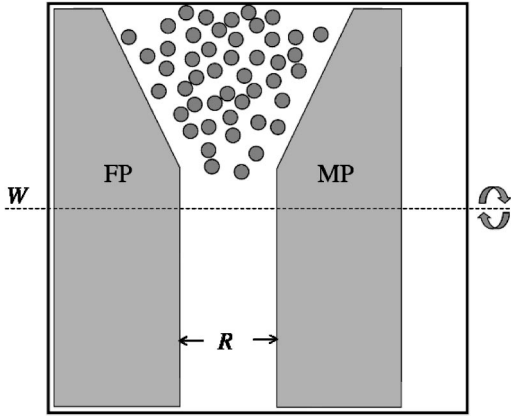


FIG. 1. Schematic diagram of the two-dimensional hopper in the upright position. The horizontal dashed line  $W$  is the axis of rotation of the rotating stage (not shown) on which the hopper is mounted.

scale in this problem is the disk diameter  $D$ , we shall express all other distances in unit of  $D$ .

### B. Jamming probability and arch vector statistics

Table I shows a brief summary of the results from our experiments. In these experiments,  $d > 1$  and we do not observe arches with only one disk, i.e.,  $N_1 = 0$ . Since the maximum extent of an arch with  $n$  disk is  $nD$ , jamming event with an  $n$ -disk arch is impossible if  $n < d$ . Hence, we observe an increasing number of  $n$ -disk arches with increasing  $d$  as indicated by the trend of the average number ( $\langle n \rangle \equiv nN_n/N_a$ ) of disks in the arch. On the other hand, most of the jamming events are contributed from only a few classes of  $n$ -disk arches.

### C. Arch vector end point statistics

From the captured images, we identify the arch and extract the position  $(-x_1, y_1)$  of the first disk from the left and the position  $(x_2, y_2)$  of the last disk, as shown in Fig. 2(b). The origin  $O$  of the co-ordinate system is at the intersection of  $L_1$  and  $L_2$ , which are, respectively, the lines passing through the points  $(-x_1, y_1)$  and  $(x_2, y_2)$  and parallel to the left and the right walls. The purpose of putting a negative sign in front of  $x_1$  is to make  $x_1$  a positive number. Because of the stochastic nature of the jamming process, the positions

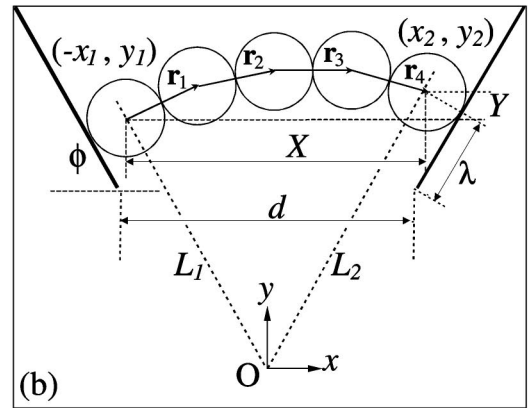
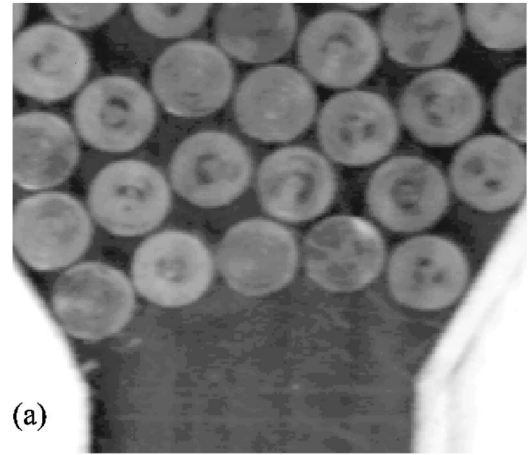


FIG. 2. An image captured (a) and its arch configuration (b) of a typical jamming event.

$(-x_1, y_1)$  and  $(x_2, y_2)$  are random variables. From the data of  $x_1$ , we get the distribution function  $F_{x_1}(\alpha)$  as the number of events with  $x_1 > \alpha$  divided by  $N_a$ . The distribution functions  $F_{\xi}(\alpha)$  with  $\xi = y_1, x_2$ , and  $y_2$  are obtained similarly.

In Fig. 3, we plot these distribution functions obtained in the experiments for  $d = 1.32$ . The insets in these figures are the density functions  $f_{\xi}(\alpha)$  that are the derivatives of their respective distribution functions  $F_{\xi}(\alpha)$  with  $\xi = x_1, y_1, x_2$ , and  $y_2$ . One can see that  $x_1$  and  $x_2$  have practically the same distribution. This feature is also apparent for  $y_1$  and  $y_2$ . This is because the hopper is symmetrical about the  $y$  axis. Fur-

TABLE I. Jamming probability  $J(d)$  and number  $N_n$  of jamming events with  $n$ -disk arch for different hopper openings  $d$ .

$d$	$N_t$	$N_a$	$J(d)$	$N_2$	$N_3$	$N_4$	$N_5$	$N_6$	$N_7$	$N_8$	$N_9$	$\langle n \rangle$
1.32	400	400	1.00	281	97	18	4	0	0	0	0	2.36
1.79	400	399	1.00	145	199	47	7	1	0	0	0	2.80
2.58	500	491	0.98	0	244	176	61	8	2	0	0	3.67
2.79	400	388	0.97	0	188	153	41	6	0	0	0	3.65
2.95	400	374	0.94	0	169	166	38	1	0	0	0	3.65
3.53	1000	713	0.71	0	0	94	440	139	40	0	0	5.18
3.74	1000	449	0.45	0	0	36	308	86	18	1	0	5.20
4.05	1000	250	0.25	0	0	0	119	89	39	2	1	5.69
4.84	1000	18	0.02	0	0	0	16	11	1	0	0	6.72

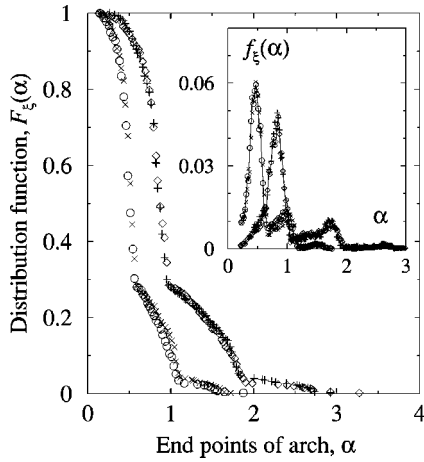


FIG. 3. Distribution functions of the end points of the arches obtained for  $d=1.32$ . The data  $\circ, \times, \diamond,$  and  $+$  are for  $F_\xi(\alpha)$  with  $\xi=x_1, x_2, y_1,$  and  $y_2$ , respectively. Their respective density functions  $f_\xi(\alpha)$  are shown in the inset accordingly.

thermore, one can see that  $F_{x_1}(\alpha)$  resembles  $F_{y_1}(\alpha)$ . Hence, we let  $\{x\}$  be the values  $\{x_1, x_2\}$  and  $F_x(\alpha)$  be the distribution function for  $x$ . Similarly, we let  $F_y(\alpha)$  denote the distribution function for  $y=\{y_1, y_2\}$ . Then we can collapse  $F_y(\alpha)$  onto  $F_x(\alpha)$  by simply rescaling  $y$  to  $y'=y/\eta$  by a numerical factor  $\eta=1.7$ , as shown in Fig. 4. Such phenomenon reflects the fact that  $(-x_1, y_1)$  and  $(x_2, y_2)$  are, respectively, points on the lines [ $L_1$  and  $L_2$  in Fig. 2(b)] parallel to the left and right walls of the hopper. Hence  $y_i=x_i \tan \phi$  for  $i=1, 2$  and the distribution of  $y$  can be scaled to that of  $x$  by taking  $y'=y/\tan \phi$ . With  $\phi=60^\circ, \tan \phi=1.73$ , this agrees very well with the numerical value (1.7) obtained from the experiment. Therefore there are only two sets of independent data out of the four measured quantities:  $x_1, y_1, x_2,$  and  $y_2$ .

**D. Arch vector components statistics**

We choose  $X \equiv x_2 + x_1$  and  $Y \equiv y_2 - y_1$  as the two independent sets of data. Let us call the displacement vector from

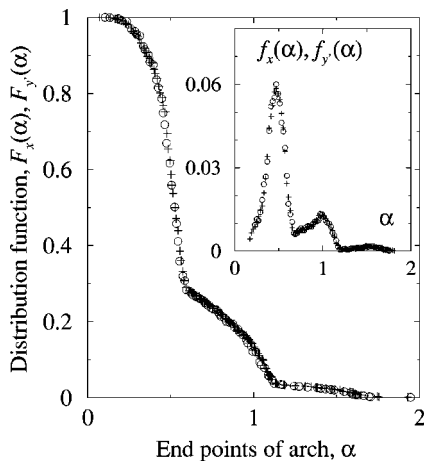


FIG. 4. Distribution function  $F_x(\alpha)$  and the scaled distribution function  $F_{y'}(\alpha)$  for  $d=1.32$  with  $y'=y/1.7$ . The inset shows the density function  $f_x(\alpha)$  and the scaled density function  $f_{y'}(\alpha)$ .

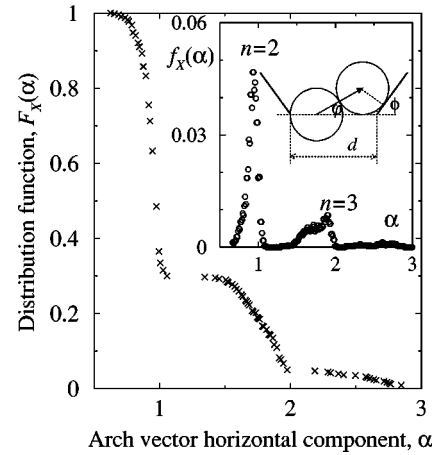


FIG. 5. Distribution function  $F_X(\alpha)$  and density function  $f_X(\alpha)$  (inset) for the horizontal component of the arch vector at  $d=1.32$ . The figure in the inset shows the geometry of the 2-disk arch when the arch vector has the shortest horizontal component.

$(-x_1, y_1)$  to  $(x_2, y_2)$  as the arch vector. Then the quantities  $X$  and  $Y$  are, respectively, the horizontal and the vertical components of the arch vector [see Fig. 2(b)]. Because of the stochastic nature of  $x_1, y_1, x_2,$  and  $y_2$ ,  $X$  and  $Y$  are stochastic too. Figure 5 shows the distribution function  $F_X(\alpha)$  and the density function  $f_X(\alpha)$  for  $d=1.32$ . One can see that  $f_X(\alpha)$  and  $f_x(\alpha)$  look similar and have the same number of peaks. However, they cannot be collapsed on each other by a simple scaling. The two main peaks in  $f_X(\alpha)$  are cleanly separated from each other, while those two main peaks in  $f_x(\alpha)$  have significant overlap. When we classify the jamming events according to  $n$ , the number of disks in the arch, we find that the first and the second peaks in  $f_X(\alpha)$  correspond to  $n=2$  and  $n=3$ , respectively. On the other hand,  $f_X(\alpha)$  is very different from the density function  $f_Y(\alpha)$  that is symmetrical about  $Y=0$  as shown in Fig. 6. This is a direct consequence of the mirror symmetry of the hopper as mentioned before.

It is worth examining the statistics in  $X$  for the 2-disk arches in which the magnitude of the arch vectors is unity.

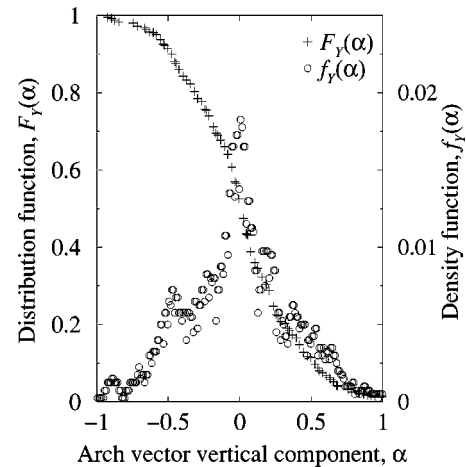


FIG. 6. Distribution function  $F_Y(\alpha)$  and density function  $f_Y(\alpha)$  for the vertical component of the arch vector at  $d=1.32$ .

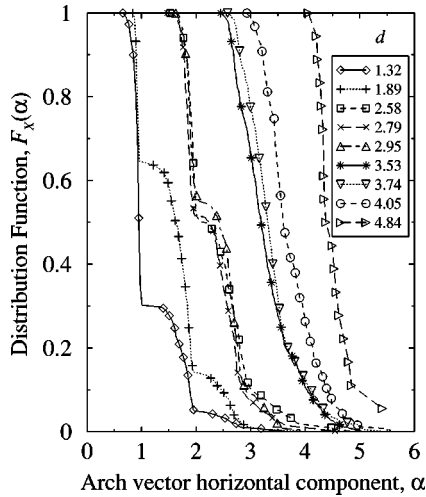


FIG. 7. Distribution function  $F_X(\alpha)$  for  $d=1.32, 1.89, 2.58, 2.79, 2.95, 3.53, 3.74, 4.05,$  and  $4.84$ . For clarity, while the lines contain all the data, the symbols represent only part of the data.

The inset in Fig. 5 indicates that the lower and upper limits of  $X$  for the 2-disk arches at  $d=1.32$  are 0.65 and 1, respectively. The upper limit of  $X$  is trivial while the lower limit of  $X$  corresponds to the situation shown in Fig. 5. This figure shows the arch vector with the maximum possible argument  $\varphi$  in a hopper with angle  $\phi$  and opening  $d$ . The geometry in this figure give  $\sin(\phi-\varphi)=(d-0.5)\sin\phi-0.5$  and the lower limit of  $X$  is then  $\cos\varphi$ . For  $\phi=60^\circ$  and  $d=1.32$ , we have  $\varphi=47.9^\circ$ . So the lower limit in  $X$  is 0.67, which is consistent with the experimental finding. However, when  $n>2$ , the lower limit of  $X$  cannot be obtained in this simple geometrical argument because the magnitude of the arch vector is no longer a constant.

### E. Effect of hopper opening on arch vector statistics

Using the arch vector concept, it is obvious that an arch with  $X<d-1$  will not survive in a hopper of opening  $d$  because such an arch will flow out of the hopper. Hence, the jamming probability  $J(d)$  should be related to the distribution function  $F_X(\alpha)$  at different  $d$ . To investigate such a relation, we examine the arch vector of each jamming event. Figure 7 shows the distributions  $F_X(\alpha)$  at  $d=1.32, 1.89, 2.58, 2.79, 2.95, 3.53, 3.74, 4.05,$  and  $4.84$ . They appear to fall into four groups according to the hopper opening. When  $d<2$  ( $d=1.32$  and  $1.89$ ),  $F_X(\alpha)$  has two sharp edges that correspond to the two peaks in their respective density function  $f_X(\alpha)$ . As mentioned before, these two peaks are contributions from the 2-disk and 3-disk arches. When  $d>2$  but less than 3, ( $d=2.58, 2.79,$  and  $2.95$ ), no 2-disk arch can be in the hopper and the contribution from the 2-disk arch vanishes. Similarly, in the third group when  $d$  lies between 3 and 4 ( $d=3.53$  and  $3.74$ ), the contribution from the 3-disk arch is zero. Finally, in the last group when  $d=4.05$  and  $4.84$ , which are greater than 4, no arches with less than five disks are observed. Qualitatively, as  $d$  increases,  $F_X(\alpha)$  changes from a steplike function to a smoothly varying function and  $f_X(\alpha)$  changes from a multi-peak function to a single-peak function

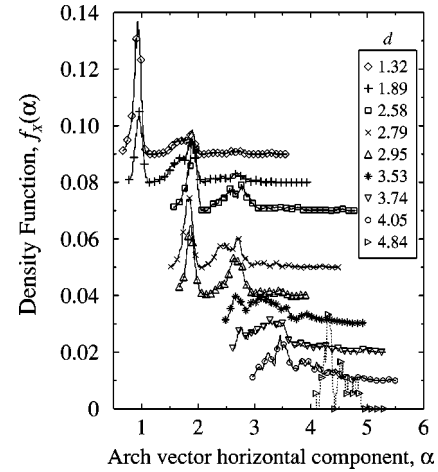


FIG. 8. Density function  $f_X(\alpha)$  for  $d=1.32, 1.89, 2.58, 2.79, 2.95, 3.53, 3.74, 4.05,$  and  $4.84$ , with their values shifted up by  $0, 0.01, 0.02, \dots, 0.08$ , respectively. For clarity, while the lines contain all the data, the symbols represent only part of the data.

as shown in Figure 8. Such trend suggests that the contributions of 2-disk arch, 3-disk arch, and 4-disk arch to  $X$  are decoupled. On the other hand, there are significant overlapping of the density functions in  $X$  for  $n$ -disk arches when  $n>4$ . The large fluctuation of the last data set ( $d=4.84$ ) is due to the small number ( $N_a=18$ ) of jamming event observed at this large hopper opening. (Fig. 8).

The change in the distribution and the density functions in  $Y$  due to increasing  $d$ , is very different from that of  $X$ . Figure 9 shows  $F_Y(\alpha)$  at different  $d$ . Surprisingly,  $F_Y(\alpha)$  does not change very much when  $d$  increases from 1.32 to 4.84. The density function  $f_Y(\alpha)$  shown in the inset of this figure is symmetrical about  $\alpha=0$ . In addition,  $f_Y(\alpha)$  peaks at  $\alpha=0$ . This implies that the arches are preferably symmetrical about the center line of the hopper. We shall return to this point later (Sec. III C) in this paper.

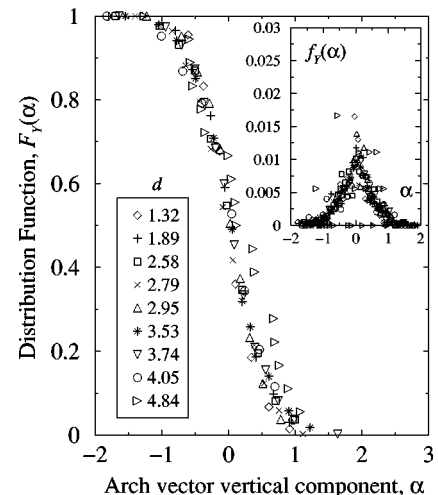


FIG. 9. Distribution function  $F_Y(\alpha)$  for  $d=1.32, 1.89, 2.58, 2.79, 2.95, 3.53, 3.74, 4.05,$  and  $4.84$ . For clarity, the symbols represent only part of the data.

### III. THE RESTRICTED RANDOM WALK MODEL

When disks are falling through the hopper, one can consider that the disks are forming arches randomly from one side of the hopper to the other side. Jamming occurs when one of these arches at the hopper opening is strong enough to block other disks from falling through. For example, in a typical jamming event shown in Fig. 2(a), it is the arch made of the lowest five disks just above the opening that stops the flow. This arch can be described by  $\mathbf{r}_1, \mathbf{r}_2, \mathbf{r}_3$  and  $\mathbf{r}_4$  where  $\mathbf{r}_i$  is the displacement vector from the center of the  $i$ th disk to that of the  $(i+1)$ th disk. While the magnitude of  $\mathbf{r}_i$  is unity, the angle  $\theta_i$  between  $\mathbf{r}_i$  and the  $x$  axis is a random variable. Hence, the  $n$ -disk arch can be considered as a trajectory of a random walker going from  $(-x_1, y_1)$  to  $(x_2, y_2)$  in  $n-1$  steps.

Although the  $\theta_i$ 's are random, there are constraints that the random walker has to follow:

$$\pi/2 > \theta_i > -\pi/2, \quad (1)$$

$$\theta_1 > \dots > \theta_i > \dots > \theta_{n-1}, \quad (2)$$

$$\forall i \neq j, \left| \sum_{k=1}^i \mathbf{r}_k - \sum_{k=1}^j \mathbf{r}_k \right| \geq 1, \quad (3)$$

$$X \equiv x_2 + x_1 > d - 1. \quad (4)$$

The first constraint (1) restricts the random walker to go from left to right only. This constraint simplifies the theoretical analysis without loss of generality because of the underlying symmetry of the hopper. The second constraint (2) means that the arch is everywhere convex. This is the mechanical equilibrium requirement for the arch to support the disks within the arch as well as those above it. The third constraint (3) is the excluded *volume* interaction among the disks. This constraint ensures that the minimum distance between any two disks in the arch is the disk diameter. The last constraint (4) selects those arches with horizontal size bigger than the hopper opening. Otherwise, the arch will fall through the hopper.

#### A. Jamming probability

Let  $f_i(\theta)$  be the probability density function for  $\theta_i$  so that the probability for  $\theta_i$  to fall between  $\beta_i$  and  $\beta'_i$  can be expressed by  $p_i = \int_{\beta_i}^{\beta'_i} f_i(\theta) d\theta$ . Then the joint probability for having a particular  $n-1$  step unrestricted random walker trajectory with  $\theta_i \in (\beta_i, \beta'_i)$  is given by the product  $p_1 p_2 \dots p_{n-1}$ . For the restricted random walker under constraint (1), the upper bound of  $\theta_1$  is  $\pi/2$ , i.e.,  $\beta'_1 = \pi/2$ . Constraint (2) requires that the maximum value of  $\theta_i$  is determined by the value of  $\theta_{i-1}$ . Hence,  $\beta'_i = \theta_{i-1}$  for  $i > 1$ . While setting the upper bounds for  $\theta_i$  is straightforward, evaluating the lower bounds  $\beta_i$  is less trivial because of the excluded *volume* effect given by constraint (3). (We shall discuss the excluded *volume* later in Sec. III B.) Nevertheless, the configuration probability density  $a_n(X)$  for an  $n$ -disk arch vector to have a horizontal component  $X$  can be written as

$$a_n(X) = A_n^{-1} \int_{\beta_1}^{\pi/2} f_1(\theta_1) d\theta_1 \int_{\beta_2}^{\theta_1} f_2(\theta_2) d\theta_2 \dots \times \int_{\beta_{n-1}}^{\theta_{n-2}} f_{n-1}(\theta_{n-1}) d\theta_{n-1} \delta\left(X - \sum_{i=1}^{n-1} \cos \theta_i\right), \quad (5)$$

where  $A_n$  is a normalization constant such that  $\int_0^\infty a_n(X) dX = 1$ .

Obviously,  $a_n(X)$  is only defined for  $n > 1$  and  $a_n(X) = 0$  if  $X > n$ . The expression for  $a_n(X)$  can be evaluated numerically if we assume that  $f_i(\theta)$  is uniformly distributed for all physical values of  $\theta_i$ . The physical values of  $\theta_i$  are determined by the excluded *volume* interaction. For  $\theta_1$ , it is the interaction with the left wall that requires  $-\phi < \theta_1 < (\pi/2) + \phi$ . Hence,  $f_1(\theta_1) = 1/\pi$  for  $\theta_1$  in this interval and zero otherwise. For  $\theta_i$  with  $i > 1$ , the constraint due to the excluded *volume* interaction between the disks is more complicated. Nevertheless,  $f_i(\theta_i)$  can be evaluated numerically. Then the probability of an  $n$ -disk arch vector with horizontal component greater than  $d-1$  can be obtained as

$$j_n(d) = \int_{d-1}^\infty a_n(X) dX. \quad (6)$$

Note that  $d-1$  is the value of  $X$  for an arch to flow through the hopper opening. The integral on  $a_n(X)$  reflects that only arches bigger than the opening can survive in the hopper, as required by constraint (4). Therefore, the jamming probability density can be written as

$$J(d) = \sum_{n=2}^\infty g_d(n) j_n(d), \quad (7)$$

where  $g_d(n)$  is the probability that the arch consists of  $n$  disks when jamming does occur. Under suitable approximation,  $g_d(n)$  can be calculated as shown in Sec. III C. It was found from experimental observation [10] that  $g_d(n)$  peaked at  $n=5$  in the narrow range when  $J(d)$  decreased from 0.9 to 0.1. When  $J(d)$  was approximated by taking only the contribution of  $n=5$ , this simple model agreed well with experiment.

#### B. Excluded volume interaction of the RRW

The RRWM described so far has little analytical results and all theoretical predictions are obtained by generating restricted random walk (RRW) trajectories under constraints (1)–(3) using Monte Carlo simulations. An analytic approximation to the RRW is needed in order to gain better insight of the jamming phenomenon. The difficulty is to calculate  $a_n(X)$  under the excluded *volume* constraint, which affects both the integrands  $f_i(\theta_i)$  and the domains of integration  $\beta_i$  in Eq. (5). Just like self-avoiding walk in polymer physics [11], the excluded *volume* interaction given by constraint (3) are hard to deal with analytically. Nevertheless, one can relax the strict condition given in Eq. (3) and one just requires the

disks to obey the “short-range” excluded *volume* interactions of three consecutive disks, as given by the constraint

$$|\theta_i - \theta_{i-1}| \leq \frac{2\pi}{3}. \quad (8)$$

These short-range excluded *volume* interactions would allow

for the overlapping of the first disk and the  $m$ th disk with  $m \geq 4$ . Relaxing the strict excluded *volume* interactions to the short-range type, one can obtain the density function  $f_i(\theta_i) = 3/4\pi$  and the lower limit  $\beta_i = \max\{-\pi/2, \theta_{i-1} - (2\pi/3)\}$  for  $i > 1$ . Ignoring the minor difference in replacing  $\beta_i$  by  $-\pi/2$ ,  $a_n(X)$  can be approximated as

$$\begin{aligned} a_n(X) &\cong A_n^{-1} \frac{1}{\pi} \int_{-\pi/2}^{\pi/2} d\theta_1 \frac{3}{4\pi} \int_{-\pi/2}^{\theta_1} d\theta_2 \cdots \frac{3}{4\pi} \int_{-\pi/2}^{\theta_{n-2}} d\theta_{n-1} \delta\left(X - \sum_{i=1}^{n-1} \cos \theta_i\right) \\ &= A_n^{-1} \frac{1}{\pi} \left(\frac{3}{4\pi}\right)^{n-2} \int_{-\pi/2}^{\pi/2} d\theta_1 \int_{-\pi/2}^{\theta_1} d\theta_2 \cdots \int_{-\pi/2}^{\theta_{n-2}} d\theta_{n-1} \delta\left(X - \sum_{i=1}^{n-1} \cos \theta_i\right) \\ &= A_n^{-1} \frac{1}{\pi(n-1)!} \left(\frac{3}{4\pi}\right)^{n-2} \int_{-\pi/2}^{\pi/2} d\theta_i \int_{-\pi/2}^{\pi/2} d\theta_2 \cdots \int_{-\pi/2}^{\pi/2} d\theta_{n-1} \delta\left(X - \sum_{i=1}^{n-1} \cos \theta_i\right), \end{aligned} \quad (9)$$

with the normalization constant  $A_n$  given by

$$A_n \equiv \int_0^\infty a_n(X) dX \cong \frac{\left(\frac{3}{4}\right)^{n-2}}{(n-1)!}. \quad (10)$$

Figure 10 shows the values of  $A_n$  calculated by Monte Carlo integration of Eq. (5) and those obtained using the analytic approximation (10). Monte Carlo results give the sum of all  $A_n$  to be  $\sum_{n=2}^\infty \approx 1.515$  while the analytic approximation gives  $\sum_{n=2}^\infty = \frac{4}{3}(e^{3/4} - 1) \approx 1.49$ . One can see that the analytic approximation is quite accurate. Hence, treating the full excluded *volume* constraint by the short-range excluded *volume* approximation produces negligible error, especially for small  $n$ . With the same approximation, we have

$$\begin{aligned} j_n(d) &\cong A_n^{-1} \frac{1}{\pi(n-1)!} \left(\frac{3}{4\pi}\right)^{n-2} \\ &\quad \times \int_{-\pi/2}^{\pi/2} d\theta_i \int_{-\pi/2}^{\pi/2} d\theta_2 \cdots \int_{-\pi/2}^{\pi/2} d\theta_{n-1} \\ &\quad \times \Theta\left(\sum_{i=1}^{n-1} \cos \theta_i + 1 - d\right). \end{aligned} \quad (11)$$

This gives

$$j_2(d) \cong \begin{cases} 1 - (2/\pi) \sin^{-1}(d-1), & d < 2 \\ 0, & d \geq 2. \end{cases} \quad (12)$$

For  $n=3$ , we have

$$j_3(d) \cong \begin{cases} 1 - \frac{4}{\pi^2} \int_0^{d-1} dy \frac{\sin^{-1}(d-1-y)}{\sqrt{1-y^2}}, & d < 2 \\ \left[1 - \frac{2}{\pi} \sin^{-1}(d-2)\right] - \frac{4}{\pi^2} \int_{d-2}^1 dy \frac{\sin^{-1}(d-1-y)}{\sqrt{1-y^2}}, & 2 \leq d \leq 3 \\ 0, & d > 3. \end{cases} \quad (13)$$

Although the analytic approximations of  $j_n(d)$  for  $n > 3$  are too complicated to be written down, their numerical values can be obtained for given  $n$  and  $d$  by generating RRW trajectories that obey constraints (1)–(4). From these trajectories, we classify the arch vectors according to  $n$  and calculate the average values for the horizontal component  $\langle X_n \rangle$  of the arch vectors in each class. For the vertical component  $Y_n$ , the average value vanishes, i.e.,  $\langle Y_n \rangle = 0$ . So we calculate the average of  $\langle |Y_n| \rangle$ . The results  $\langle X_n \rangle$  and  $\langle |Y_n| \rangle$  for

$d=3.74$  and  $4.05$  are plotted in Fig. 11 along with the experimental results for comparison. The theoretical values of both  $\langle X_n \rangle$  and  $\langle |Y_n| \rangle$  increase with  $n$ . The experimental data also show the general trend of increasing with  $n$  except for the data for large  $n$  where the experimental data are only from one sample due to the fact that arch with large  $n$  is very improbable. Furthermore, the predicted values of both  $\langle X_n \rangle$  and  $\langle |Y_n| \rangle$  agree well with the experimental data. Since there is no fitting parameter in the theoretical values, our results

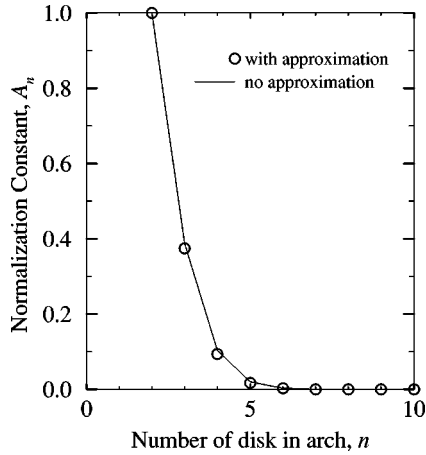


FIG. 10. Comparison of the normalization constant  $A_n$  calculated using the short-range excluded *volume* approximation (solid line) calculated by using Eq. (10) and those ( $\circ$ ) that are obtained using direction Monte Carlo simulation with no approximation.

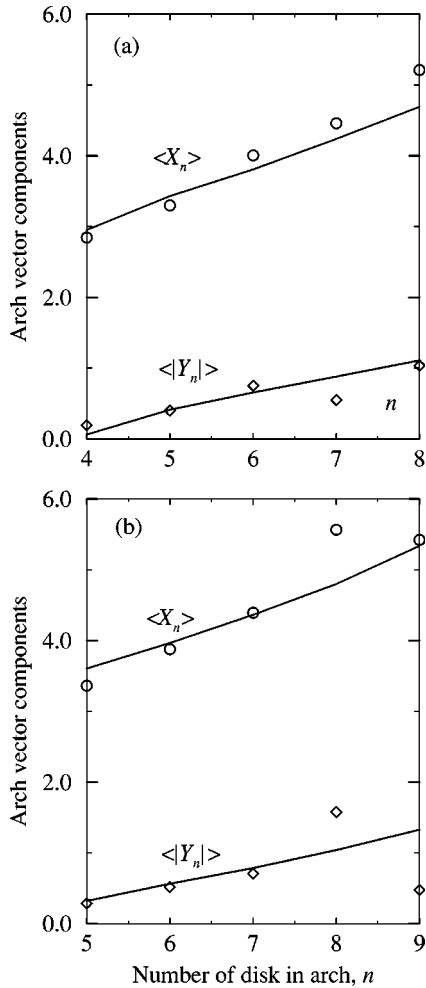


FIG. 11. Average values of the horizontal component ( $\circ$ ) and the vertical component ( $\diamond$ ) of the  $n$ -disk arch vector from experiments for  $d=3.74$  (a) and  $4.05$  (b). The lines are the theoretical values obtained from RRW trajectories generated by Monte Carlo simulations.

indicate that the RRW model can capture the configuration of the arch quite accurately.

### C. Circular arch approximation

It should be pointed out that the normalization constant  $A_n$  equals  $j_n(1)$  that is the probability of getting an  $n$ -disk stable arch from a collection of disks with excluded *volume* interactions, regardless of the value of  $X$ . Hence, one can treat  $A_n$  as the stability probability of an  $n$ -disk arch. The exponential decay form in Eq. (10) reveals that  $n$ -disk arches with large  $n$  are highly improbable. Using the stability probability  $A_n$ , further theoretical calculations concerning the statistics of the arches in the jamming state can be obtained by approximating the shape of the jamming arch. Motivated by the experimental observation that the distribution in  $Y$  peaks at  $Y=0$  and hence the jamming arches are preferably symmetric, we take the bold assumption that the jamming arch can be approximated by a circular arc centered at the apex of the hopper cone. Suppose the arch begins at a distance  $\lambda$  from the opening on the hopper wall, the circular arc length is given by  $\ell = (2\lambda + d \sec \phi)[(\pi/2) - \phi]$ . Then the number of disks in the arch can be approximated as  $n = \lceil \ell \rceil$ , which is the integer just larger than  $\ell$ . Assuming that  $\lambda$  is uniformly distributed in the region  $[0, \infty]$ , arches with different values of  $n$  can be generated. Of course, arches with large values of  $n$  is improbable due to stability and  $A_n$  will account for this effect. Thus the information about the arch statistics can be calculated by generating  $n$  in a simulation. Denote the number of arches with  $n$  by  $M_n$ , then  $g_d(n)$  can be calculated as

$$g_d(n) = \frac{A_n M_n}{\sum_n A_n M_n}. \quad (14)$$

Figure 12 shows the theoretical predictions for  $g_d(n)$  using the circular arc model together with the experimental results for comparison. The theoretical predictions can capture all the qualitative features of  $g_d(n)$  and even agree quantitatively quite well in some cases.

The mean disk number  $\langle n \rangle$  in the jamming arches can also be computed as  $\langle n \rangle = \sum_n n g_d(n) / \sum_n g_d(n)$ . The theoretical results together with the experimental data are shown in Fig. 13. The experimental data points all lie roughly near the predicted curve. It is worth noting that the theoretical curve of  $\langle n \rangle$  increases monotonically with  $d$  with kinks for values of  $d$  slightly less than integral values where the increase of  $\langle n \rangle$  becomes very slow. Such a behavior also seems to appear in the experimental data near  $d \lesssim 3$  and  $d \lesssim 4$ . However, more sample statistics are required to firmly establish this.

## IV. SUMMARY AND OUTLOOK

In this paper, the experimental results on the detail statistics of the jamming arches in a two-dimensional hopper are reported. The distribution functions of the end positions of the jamming arches are measured and the statistics of the jamming arches are obtained. The flow of granular particle in

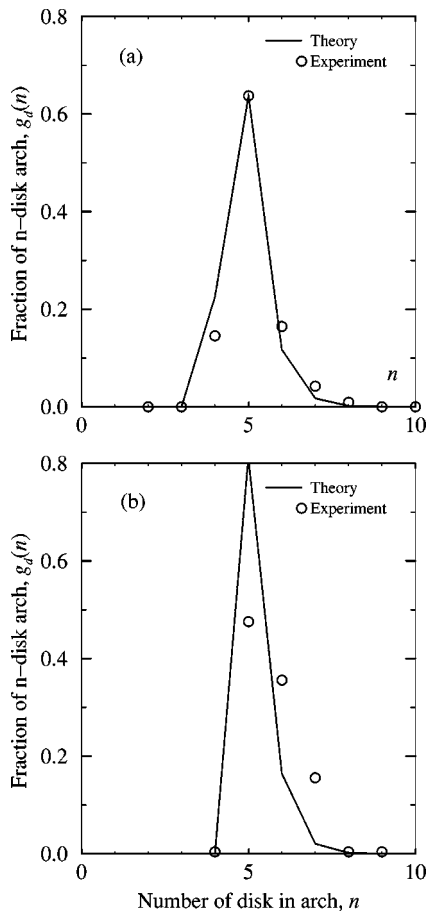


FIG. 12. Fraction of  $n$ -disk arches in jamming events  $g_d(n)$  for  $d=3.75$  (a) and  $4.05$  (b). The “○”s are from experimental observation and the lines are from theoretical calculation using the circular arch approximation.

the hopper near the jamming region is a complicated dissipative process. We attempted to model such a complex phenomenon with a stochastic approach using a simplified restricted random walker model that bears basically only excluded *volume* interaction and stability conditions. Despite its simplicity, the RRWM captures most of the essential characteristics of the jamming arches even quantitatively. With the further theoretical analysis of the RRWM together with

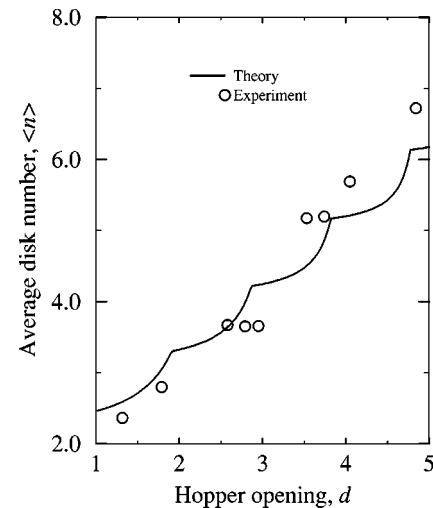


FIG. 13. The variation of the mean number of disks  $\langle n \rangle$  in the jamming events with the hopper opening  $d$ . The “○”s are from experimental data and the line is from theoretical calculation.

the circular arch approximation, much insight concerning the probability of forming a jamming arch can be found. In particular, detailed arch statistics, such as  $g_d(n)$  and the mean number of disks in a jamming arch can be calculated, which agrees quite well with experimental measurements.

In practical applications, there are of course many more complications in hoppers, such as the friction and adhesion among the grains, which would increase the jamming probability. Our RRWM could be extended to include such effects by locally relaxing the convexity constraint to some extent. Other interesting effects in the jamming phenomena, such as grain polydispersity, effects of irregular grain shapes, asymmetric hopper, and replacing disks by spheres are currently under our experimental investigations. These results will be presently elsewhere.

#### ACKNOWLEDGMENTS

The authors would like to thank Professor H. K. Pak (Pusan National University, Korea) who initiated our study on the jamming phenomenon of granular flow. This research was supported by the National Council of Science of Taiwan under Grant Nos. NSC 90-2112-M-001-034 and 90-2112-M-008-037.

[1] R.M. Nedderman, U. Tuzun, S.B. Savage, and G.T. Houlby, *Chem. Eng. Sci.* **17**, 1597 (1982).  
 [2] P.Y. Lai, L.C. Jia, and C.K. Chan, *Phys. Rev. Lett.* **79**, 4994 (1997).  
 [3] L.C. Jia, P.Y. Lai, and C.K. Chan, *Phys. Rev. Lett.* **83**, 3832 (1999).  
 [4] L.C. Jia, P.Y. Lai, and C.K. Chan, *Physica A* **281**, 404 (2000).  
 [5] Wei Chen, Meiyang Hou, Kunquan Lu, Zehui Jiang, and Lui Lam, *Phys. Rev. E* **64**, 061305 (2001).  
 [6] J.C. Tsai, W. Losert, G.A. Voth, and J.P. Gollub, *Phys. Rev. E*

**65**, 011306 (2002).  
 [7] W.A. Beverloo, H.A. Leniger, and J. Van de Velde, *Chem. Eng. Sci.* **15**, 260 (1961).  
 [8] H.M. Jaeger, S.R. Nagel, and R.P. Behringer, *Rev. Mod. Phys.* **68**, 1259 (1996).  
 [9] G. Ristow, *Pattern Formation in Granular Materials* (Springer, New York, 2000).  
 [10] Kiwing To, Pik-Yin Lai, and H.K. Pak, *Phys. Rev. Lett.* **86**, 71 (2001).  
 [11] P.G. de Gennes, *Scaling Concept in Polymer Physics* (Cornell University Press, Ithaca, NY, 1979).